ISSN: 2476-6909; Modares. Mech. Eng. *2025;25(09):603-611.*

Modares Mechanical Engineering

DOI: 10.48311/mme.2025.27796
journal homepage: mme.modares.ac.ir

Molecular Dynamics Simulation of Induced Shear Stress on Cell Membrane

Alireza Lotfalinezhad, Afsaneh Mojra*

Department of Mechanical Engineering, K. N. Toosi University of Technology, Tehran, Iran

ARTICLE INFO

Article Type
Original Research

ABSTRACT

Targeted drug delivery has been a major advancement in modern medicine, with a specific focus on delivering therapeutic drugs directly to diseased tissues as a means of minimizing side effects. A basic concern especially at the cellular level is drug carrier interaction with biological membranes under mechanical forces. On the contrary to latter researches, it is well important to investigate drug delivery mechanism in atomic scale environment. A critical parameter in determining the success of drug delivery is the degree of drug carrier and biological membrane interaction under mechanical stresses. Therefore, in the current study, molecular dynamics (MD) simulations were carried out to examine the biomechanical response of membranes at the nanoscale level. In order to investigate the effect of blood flow over cell membrane and its permeability, the outer membrane of a cell was modeled using a POPC lipid bilayer and shear strain and stress were evaluated. The impact of variation in blood flow velocity—such as those induced by physiological changes like aortic stiffening, calcification, or pathological conditions—was evaluated on the induced shear stress. The given results implied that as velocity increased, the shear stress approached permissible limit for different blood vessel types. Notably, at a velocity of 5 m/s, shear stress reached critical levels, nearing the structural threshold beyond which membrane rupture could occur. Such extreme conditions have direct implications for vascular biomechanics, as excessive shear stress may compromise membrane stability and disrupt essential cellular functions, particularly in circulatory environments exposed to fluctuating hemodynamic forces.

Article History
Received: July 04, 2025
Accepted: September 13, 2025
ePublished: November 01, 2025

Keywords: Molecular Dynamics (MD); Large-scale Atomic/Molecular Massively Parallel Simulator (LAMMPS); Shear Stress; Cell Membrane; Permeability.

How to cite this article
Lotfalinezhad A.R, Mojra A, Molecular Dynamics Simulation of Induced Shear Stress on Cell Membrane. Modares Mechanical Engineering; *2025;25(09):603-611*.

**Corresponding author's email: mojra@kntu.ac.ir*
**Corresponding ORCID ID: 0000-0001-8790-7016*

1- Introduction

In the management of solid neoplasms, the standard therapeutic approach often involves the administration of chemotherapeutic agents. These agents are characterized by their low molecular weight and diminutive size, typically measuring a few nanometers in diameter, which facilitates their cytotoxic activity. Targeted drug delivery is a strategic approach designed to enhance the concentration of pharmacological agents within specific body regions. The objective is to amplify the therapeutic impact on targeted tissues, thereby optimizing the efficacy of treatment. Concurrently, this method aims to diminish the drug's presence in non-targeted tissues, which significantly curtails the spectrum of potential side effects. Extensive research has focused on improving drug delivery mechanisms to maximize therapeutic efficacy. Notably, Byron [1] discussed devices aimed at enhancing the efficiency of lung drug delivery. He argued that although achieving high delivery efficiencies is possible, the development of such devices is expensive and may only be justified if paired with drugs that significantly benefit therapeutically and economically from the investment. Additionally, selecting an appropriate device requires careful consideration of the physicochemical properties and dosing requirements of the drug intended for inhalation. This approach differs from conventional drug targeting methods, which primarily rely on the biochemical and physicochemical characteristics of diseased tissue.

Shear-targeted drug delivery is an innovative approach that takes advantage of the unique physical conditions present in diseased blood vessels. In healthy arteries, the hemodynamic conditions tend to remain quite stable. The average shear stress in a healthy arterial system is about 1.5 pascals (Pa), which helps to maintain normal physiological function. In contrast, a blood vessel with stenosis can exhibit shear stress ranging from 15 to 100 Pa [2]. Wall stress increases nonlinearly with blood pressure, particularly with pulse pressure [3]. Shear stress acting parallel to the surfaces of the artery's layers—intima, media, and adventitia—can lead to interlayer sliding, which plays a significant role in arterial biomechanics [4]. This effect depends on blood pressure and the distinct mechanical properties of each layer [5]. The shear stress caused by blood flow is essential in vascular pathophysiology. Table 1 summarizes shear stress values in human vessels [6]. Shear stress influences endothelial cell behavior, gene expression, platelet and red blood cell aggregation, and vascular wall remodeling, among other critical biological processes [7].

Biocompatible and biodegradable polymers are extensively employed in clinical settings for controlled drug release. The global market for these polymer-based systems is valued at approximately $60 billion annually, benefiting over 100 million patients each year [8]. A drug-release system delivers the active substance to the patient. Initially, a diffusion mechanism ensures sustained drug release, followed by bulk hydrolysis of the polymer, making it ideal for delivering relatively small molecules. However, modern techniques necessitate the incorporation of drugs that vary in nature and molecular size, and diffusion alone is insufficient for releasing large molecules [9]. Natural polymers such as arginine, chitosan, dextrin, polysaccharides, and hyaluronic acid have been utilized in polymeric drug delivery systems. The micro-processes required for developing such carriers—including genetic engineering and in vivo treatments to incorporate therapeutic substances—make it challenging to maintain the integrity of both natural and synthetic polymers within the body. Traditionally, there has been a significant gap between synthetic and biological systems [10]. The first closed bilayer phospholipid systems, known as liposomes, were described in 1965 and were soon proposed as drug delivery systems. Advances in phospholipid systems led to numerous clinical trials in various fields, including the delivery of anti-cancer drugs [11]. Currently, liposomes are the most widely used system for delivering antimicrobial drugs and can release their payloads to cell membranes or into the interior of bacteria. The unique structure of liposomes, featuring a lipid membrane surrounding an aqueous cavity, allows them to carry both hydrophobic and hydrophilic compounds without chemical modification [12].

Nanoparticles, typically up to 100 nanometers in size, are small objects used in drug transport and therapeutic applications. They enable targeted drug delivery and controlled release. The European Medicines Agency (EMA) defines nanomedicines as drugs composed of nanomaterials. Various nanomedicines have been developed and applied in both clinical and non-clinical areas. These nanomedicines are classified into several categories, including liposomes, quantum dots, polymeric micelles, carbon nanotubes, and fullerenes [13]. Nanoparticles have proven beneficial in diagnosis, treatment, and surgeries by improving drug stability in the body, protecting drug molecules within systemic circulation, and ensuring controlled and sustained drug release to specific sites [14]. Nanoparticles are highly reactive entities with unique physicochemical properties, including a small, controllable size and a large surface-to-mass ratio [15]. These characteristics enhance the suitability of drug molecules for targeted delivery by improving their pharmacokinetic and pharmacodynamic properties [16].

The use of molecular dynamics (MD) in targeted drug delivery systems has been an attractive research topic during recent years. Notably, Pastor et al. [17] evaluated the performance of the CHARMM36 (C36) and CHARMM27 (C27) lipid force fields and POPC (palmitoyl-oleoyl-sn-glycero-phosphocholine) bilayers using the TIP3P water model. The simulations demonstrated that C36 and C27 accurately reproduce several key membrane properties, including headgroup area. The headgroup area for POPC was found to be within 5% of experimental values, indicating good agreement. However, there are certain limitations. Remarkably, the calculated membrane dipole potential (MDP) for POPC bilayers was higher than experimental estimates [17]. In a study by Murzyn et al. [18], the presence and configuration of unsaturated bonds in phospholipid acyl chains and their influence on the structural and interfacial properties of lipid bilayers were examined using molecular dynamics simulations. Bilayers composed of POPC, PEPC, and DMPC were analyzed, and the key finding was that the average area per phosphatidylcholine (PC) molecule was approximately 4 $Å^2$ larger in the mono-unsaturated POPC and PEPC bilayers compared to the saturated DMPC bilayer. These structural properties can influence membrane fluidity and permeability, highlighting

the critical role of lipid unsaturation in determining membrane behavior [18].

Nanobubbles—gas-filled vesicles typically under 1 μm—can be engineered to carry therapeutic agents and release them at specific sites. Shear stress plays a crucial role in modulating the endothelial cell response to nanobubbles. Under elevated shear conditions, endothelial cells can alter membrane permeability, making them more receptive to nanobubble-mediated delivery, especially when combined with ultrasound or other mechanical stimuli. Numerical simulations were carried out using molecular dynamics (MD) and computational fluid dynamics (CFD) on encapsulated bubbles to evaluate the impact of water jets on adjacent walls. The resulting stress and pressure imposed on the wall were reported accordingly [19,20]. In several recent studies [21–23], the collapse of cavitation bubbles was investigated to generate strong flow fields that resulted in cell detachment from the substrate and temporary membrane poration. However, the main limitation of these studies is the absence of molecular-level resolution regarding membrane disruption mechanisms.

The molecular dynamics in nanobubble-mediated drug delivery has been addressed in a few studies. Among them, Vedadi et al. [24] investigated the effect of nanobubble size and velocity on cell membranes. They suggested that the collapse of nanobubbles near biological membranes can create transient nanopores due to the impact of nanojets. This phenomenon has potential applications in targeted drug delivery, as it could facilitate the transport of therapeutic agents across cell membranes. Despite these findings, the study focused on a pure water system without considering biologically relevant interfaces such as lipid membranes or solutes, while using the ReaxFF potential. Sun et al. [25] employed MD simulations to explore how lipid-shelled nanobubbles interact with phospholipid bilayers under shock wave conditions. The simulations revealed that both the initial diameter of lipid nanobubbles and the velocity of the applied shock wave significantly affect the collapse dynamics. The study also compared lipid nanobubbles with vacuum nanobubbles and found that lipid-coated nanobubbles attenuate the effects of shock waves more effectively. Nan et al. [26] investigated the mechanisms by which shock-induced nanobubble collapse leads to the perforation of cellular membranes. Using Martini coarse-grained MD simulations, they explored the formation and evolution of nanoscale cavitation during this process. Unlike related studies, this work focused on coarse-grained MD, which is computationally efficient but may overlook critical atomistic details of lipid–drug or lipid–solvent interactions during nanobubble collapse.

Table 1 Wall shear stress in normal and stenotic human vessels

Blood Vessel	Wall Shear Stress (Pa)
Normal arteries	1-6
Normal veins	0.1-1
Mildly Stenotic arteries	>10
Highly Stenotic arteries	>100

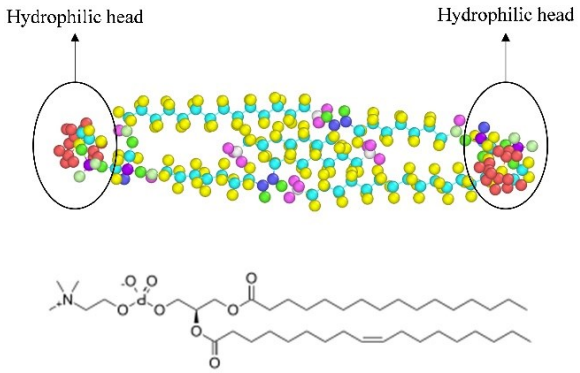

Fig. 1 Molecular Structure and Chemical Formula of POPC Lipid Bilayer

In the present study, we performed MD simulations to investigate the shear stress exerted on the cell membrane under conditions similar to blood flow. The novelty of this study lies in understanding how mechanical forces generated by blood flow influence the cell membrane at the molecular level. A particularly innovative aspect of our research was the exploration of how variations in blood flow velocity—such as those induced by physiological changes like aortic stiffening, calcification, or pathological conditions—alter both the magnitude and spatial distribution of shear stress on the membrane surface. These factors are known to contribute to cardiovascular diseases, yet their direct impact at the molecular scale of the cell membrane has remained unclear.

2- Model description

In this study, POPC (palmitoyl-oleoyl-sn-glycero-phosphocholine) lipid was utilized to simulate the cell membrane. The geometric and chemical structures of POPC are illustrated in “Figure 1”. To examine the interaction between POPC and the predominant body fluid, water, the lipid was combined with water molecules. According to this figure, the structure includes three main regions: the hydrophilic (water-attracting) headgroup, the glycerol backbone, and the two hydrophobic (water-repelling) fatty acid tails. The headgroup, made up of atoms like phosphorus, nitrogen, and oxygen, interacts with the surrounding water. The two tails differ slightly—one is saturated (straight) and the other is unsaturated (kinked)—which influences how the molecule packs in a membrane and affects its fluidity. These POPC monomers are arranged into a bilayer structure, mimicking a cell membrane in an aqueous environment.

"Figure 2" illustrates an MD simulation snapshot of a fully assembled POPC lipid bilayer, constructed by replicating individual POPC monomers. The bilayer is presented in a space-filling representation, with each colored sphere corresponding to a specific atom type. The outer surfaces display the lipid headgroups, composed of various polar atoms oriented toward the aqueous environment, effectively mimicking the natural arrangement found in biological membranes. This bilayer serves as a model of a semi-permeable membrane system, allowing for the investigation of its structural integrity and permeability under external mechanical perturbations. The dense packing of the hydrophobic tails contributes to the membrane’s mechanical stability, while the relatively disordered headgroup regions provide fluidity and adaptability. This configuration enables

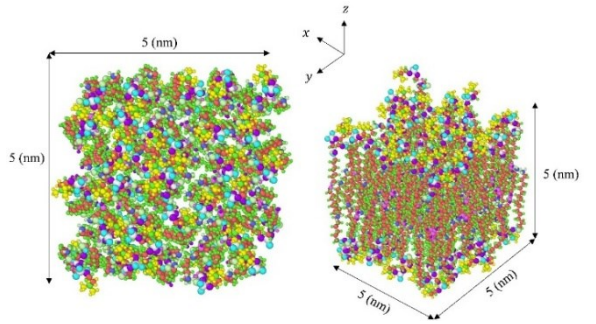

Fig. 2 Simulation snapshot of a POPC lipid bilayer in a space-filling representation, showing the organized assembly of lipid molecules with hydrophilic headgroups facing the aqueous environment and hydrophobic acyl chains forming the membrane core. This model system is used to study membrane structure, stability, and permeability under shear-induced mechanical stress.

detailed analysis of transient pore formation, molecular transport across the bilayer, and the mechanisms underlying membrane disruption.

The simplified POPC bilayer model, while useful for controlled molecular dynamics studies, differs significantly from real biological membranes in several key ways. Unlike the diverse and asymmetric lipid composition of natural membranes, POPC systems are uniform and symmetric, lacking cholesterol, membrane proteins, and environmental complexity. This simplification leads to an overestimation of membrane fluidity and overlooks critical phenomena such as lipid rafts, protein–lipid interactions, and electrostatic gradients. Despite these limitations, POPC remains a valuable baseline for probing fundamental membrane behavior prior to introducing biological realism.

"Figure 3" presents a molecular dynamics simulation configuration depicting a POPC lipid bilayer overlaid with a layer of water molecules. The entire simulation box measured 5 × 5 × 10 nm, and periodic boundary conditions were applied in all directions. Within this simulation domain, a total of 7906 POPC lipid atoms were in contact with 6707 water molecules. The overlying water molecules are distinctly represented by red and white spheres, corresponding to oxygen and hydrogen atoms, respectively. This configuration reproduces a biologically relevant environment, where the membrane exists in direct contact with an aqueous medium, essential for accurately modeling cellular conditions. The system is designed to investigate the effects of shear stress induced by directional water flow across the membrane surface. By applying controlled velocities to the water molecules, mechanical forces are transmitted to the lipid headgroups, enabling the study of stress propagation and deformation within the membrane.

The simulation setup shown in "Figure 3" was performed in two main steps. First, the simulation geometry of "Figure 3" was equilibrated using the NVE ensemble for 300 picoseconds. Subsequently, the flow velocity (implemented to all the water molecules) was changed and applied according to the NVT set at a base temperature of 38°C (310 K), and the shear stress on the cell membrane surface was calculated accordingly. The water model employed in this simulation was TIP3P and considered as rigid bodies during the simulation. The simulation time step was set to 2 femtoseconds, and the CHARMM force field was used.

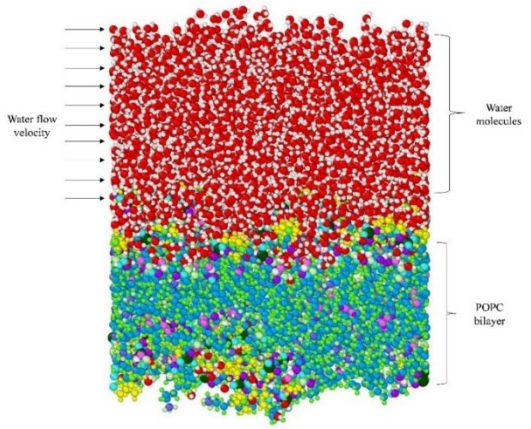

Fig. 3 Simulation snapshot showing a POPC lipid bilayer overlaid with a layer of water molecules. This configuration is used to study the effects of shear stress on the membrane by applying velocity to the water layer, allowing investigation into membrane deformation, permeability changes, and lipid structural responses under fluid-induced mechanical forces

Table 2 pairwise interactions of water molecules based on TIP3P model

	O-O	H-H
ϵ ($^{kCal}/_{mol}$)	0.1521	0.046
σ (nm)	0.315	0.04

The interaction coefficients between water and the cell membrane, based on the Lennard-Jones potential (Eq. 1), were calculated by Lorentz-Berthelot law.

$$V_{LJ}(r) = 4\varepsilon[\left(\frac{\sigma}{r}\right)^{12} - \left(\frac{\sigma}{r}\right)^{6}] \quad (1)$$

The simulated cell membrane measured 5 x 5 x 5 nanometers and comprised 59 monomers of the POPC lipid structure. In total, the cell membrane's geometry included 7,907 atoms. Boundary conditions on x, y and z direction were periodic and large enough to ensure the geometry equilibration. To simulate the extracellular environment, the upper region of the membrane was filled with water molecules, as previously detailed. This region contains a total of 10,400 water molecules. "Table 2" presents the pairwise interaction coefficients of water molecules based on the Lennard-Jones potential. The coefficients of (Equation 1) for interactions between hydrogen and oxygen atoms may vary between models, depending on the specific model used. The corresponding and values from the Lennard-Jones potential can be determined using various methods, such as the Lorentz-Berthelot law [27]. It is notably to say that all simulations were conducted via LAMMPS (Large-scale Atomic/Molecular Massively Parallel Simulator) package and also geometries were built by using VMD (Visual Molecular Dynamics).

The impact of variations in blood flow velocity—such as those induced by physiological changes was stusied on the cell membrane. It is well known the velocity distribution in blood vessels is categorized into the following three types [28]:

- Mild velocity increase resulting from mild aorta stiffening: v < 2 m/s
- Moderate velocity increase resulting from moderate aorta stiffening: 3 m/s < v < 4 m/s
- Severe velocity increase resulting from extreme aorta stiffening: v > 4 m/s

3-Results and Discussion

High velocities in blood vessels are attributed to the presence of calcium deposits. In order to examine the effect of velocity distribution on cell membrane, we presented the shear strain distribution contours and the shear stress per unit time graph on the simulated cell membrane, resulting from the application of each velocity for duration of 350 picoseconds. Since the imposed velocity values are constant and the velocity profile remains uniform along the simulation domain, shear stress fluctuations do not change significantly with increased simulation time. Currently, shear stress values are averaged over a sufficiently long simulation period (350 picoseconds), ensuring that the findings of this study are reliable.

"Figure 4" illustrates the time-dependent temperature changes, while "Figure 5" depicts the energy changes of the entire system per unit time. According to the graph, the energy has reached an equilibrated state, indicating that the geometry is stable.

"Figure 4" illustrates the temporal evolution of the temperature of a POPC lipid bilayer subjected to wall shear stress, as calculated from MD simulations. The x-axis denotes the simulation time (up to 300 picoseconds), while the y-axis represents the corresponding membrane temperature in degrees Celsius. An initial rapid increase in temperature is observed within the first ~50 picoseconds, rising from approximately 25 °C to nearly 38 °C. This behavior indicates a swift energy transfer from the sheared fluid to the membrane, likely resulting from viscous dissipation and interfacial molecular interactions. Following the initial rise, the temperature exhibits a slower, more gradual increase, reaching a maximum of slightly above 40 °C around 150 picoseconds. After this peak, the temperature begins to equilibrate, with minor fluctuations suggesting a dynamic equilibrium state. These variations may be attributed to transient molecular rearrangements within the lipid bilayer and continued, albeit less intense, energy exchange with the surrounding fluid. The overall trend suggests that the POPC membrane responds sensitively to externally applied shear, with its thermal profile reflecting the interplay between fluid-induced stress and internal dissipative mechanisms.

"Figure 5" presents the total energy profile of the POPC lipid bilayer system subjected to shear flow over 300 picoseconds. The y-axis denotes the total energy in kcal/mol, while the x-axis represents the simulation time in picoseconds. A sharp decrease in total energy is observed during the initial 25–30 picoseconds, indicating a rapid relaxation of the system as it transitions from its initial configuration toward a more thermodynamically stable state. Following this initial energy drop, the system exhibits minor fluctuations around an average value, with the total energy eqilibrationn at approximately −18234 kcal/mol. These small oscillations suggest local structural adjustments within the membrane or transient interactions between the lipid and water molecules under shear stress. The relative constancy of total energy over the remaining simulation time confirms that the system reaches a quasi-equilibrium state despite the imposed mechanical perturbation. This behavior reinforces the thermal data, indicating that the POPC bilayer retains structural and energetic stability under steady-state shear

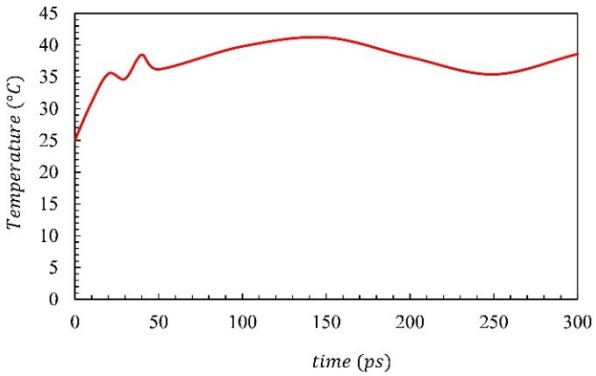

Fig. 4 Temperature evolution of the POPC lipid bilayer under shear stress over a 300 picoseconds molecular dynamics simulation. The temperature increases rapidly during the early stages due to energy transfer from the sheared water molecules, followed by gradual stabilization, indicating thermal equilibration of the membrane

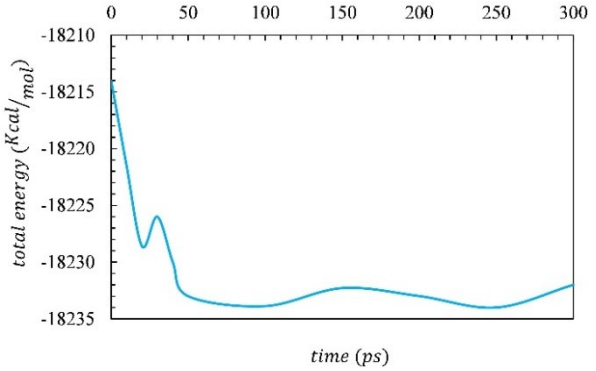

Fig. 5 Total energy profile of the POPC membrane system subjected to shear-induced flow. A significant initial decrease in total energy reflects system relaxation, followed by minor fluctuations around a stable value, suggesting attainment of a quasi-equilibrium state

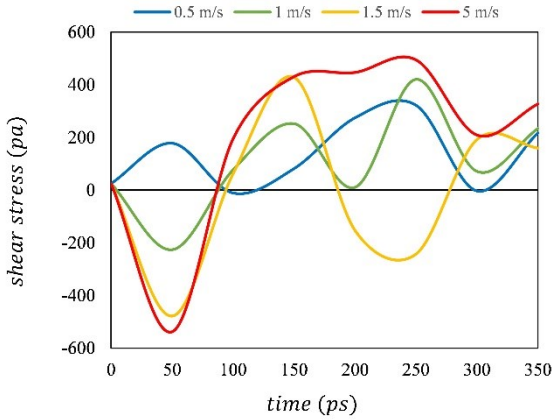

Fig. 6 Shear Strain Distribution in POPC Membrane Under Fluid Interaction A visualization of localized strain in the lipid bilayer, highlighting spatial variations in deformation due to imposed shear forces.

conditions, a critical characteristic for biological membranes exposed to fluid flow environments.

According to [17], the CHARMM force fields C27 and C36 were evaluated for their applicability to the POPC phospholipid bilayer of the cell membrane. By comparing the simulation results with experimental data, it was conclusively determined that the C27 force field is suitable for modeling the POPC monomer within the cell membrane. Based on these findings, the C27 force field was employed in this study to simulate the cell membrane for the case illustrated in "Figures

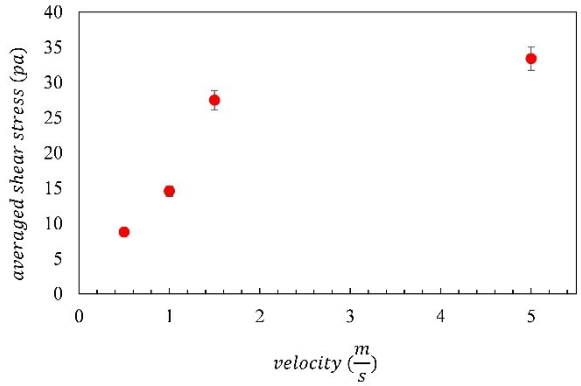

Fig. 7 Shear Stress Distribution in POPC Membrane Under Varying Fluid Velocities A visualization of shear strain variations within the lipid bilayer, demonstrating the impact of increasing fluid velocity on membrane deformation.

2 and 3". As illustrated in "Figure 6", an increase in tangential velocity on the plane, corresponding to an increase in water molecule velocity, leads to a proportional rise in the amplitude of shear stress oscillations. The results indicate that lower velocities, such as 0.5 m/s and 1 m/s, exhibit reduced oscillation amplitude compared to higher velocities like 1.5 m/s and 5 m/s. This trend highlights the direct relationship between fluid velocity and shear stress impact on membrane mechanics.

"Figure 7" provides the average shear stress values for each tested velocity over 300 picoseconds of simulation time. The results indicate that at a velocity of 5 m/s, classified within the severe velocity range, shear stress exceeds the permissible and tolerable limits. This excessive shear stress can potentially lead to structural failures or adverse effects within the membrane. Shear stress was calculated along the x-y axis of the membrane plane, with velocities spanning both moderate and severe ranges. The findings from "Table 1" and "Figure 7" consistently demonstrate that as fluid velocity increases, the membrane approaches its permissible shear stress limit, reinforcing the validity of the results.

"Figures 8" present the shear strain distribution contours for each velocity. The images indicate that the shear strain increases eith the tangential velocity on the cell membrane. This results in a gradual increase in cell permeability over time. If the velocity exceeds the allowable limit, it may lead to the rupture of the cell membrane. According to the results reported in "Table 1", the allowable limit for the blood vessels examined in this study is 100 Pascal. In "Figure 8-a", the distribution of shear strain (Eq 2) in the early phase of the simulation box is shown. Based on this illustration, the shear strain at t = 0 picoseconds is close to 0. It should be noted that in the subsequent stages of the simulation, the desired velocity was applied to the water molecules according to "Figure 3".

$$\gamma_{xy}^{(i)} = \frac{\partial u_x^{(i)}}{\partial y} \tag{2}$$

Additionally, the shear stress and shear strain values discussed in this article were calculated and reported accordingly

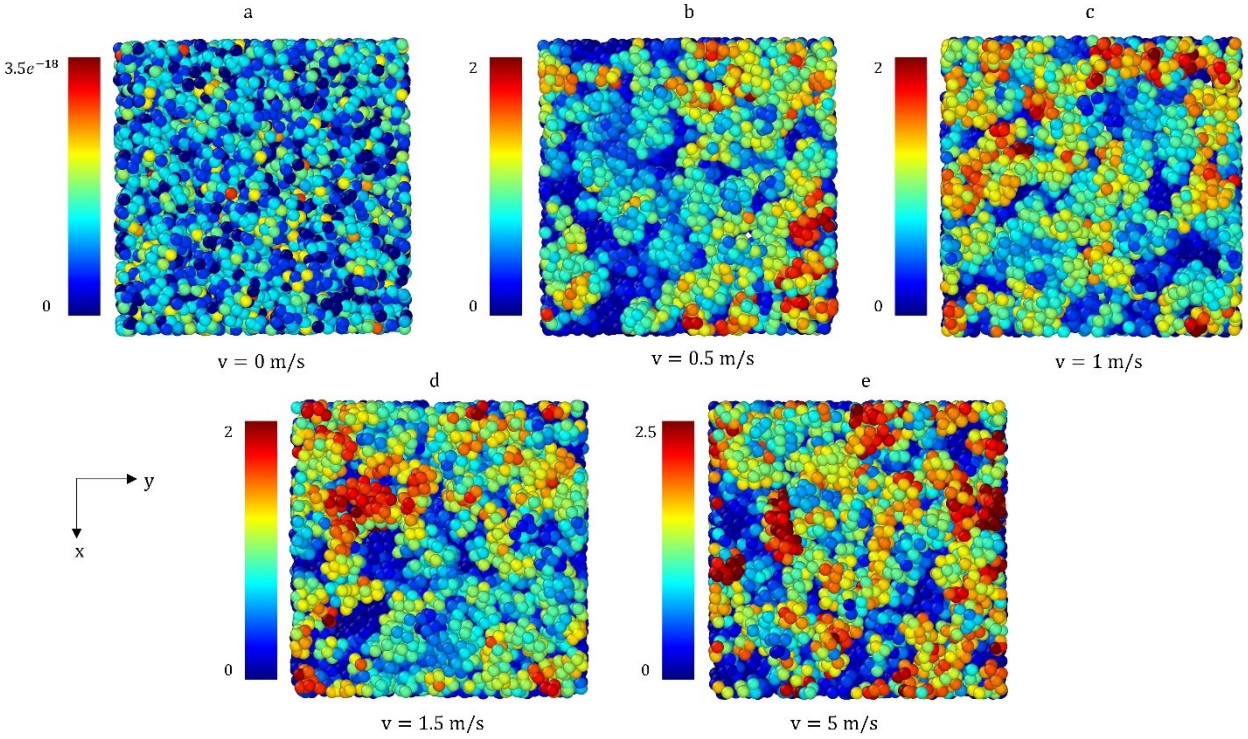

Fig. 8 Contour plots depicting the spatial distribution of shear strain exerted by water across a POPC lipid bilayer under different applied shear rates along the membrane plane. Shear conditions were applied with magnitudes of (a) v = 0 m/s, (b) v = 0.5 m/s, (c) v = 1.0 m/s, (d) v = 1.5 m/s, and (e) v = 5.0 m/s. The resulting shear stress fields captured at 200 picoseconds after the initiation of simulation setup, highlight the membrane–fluid interface dynamics. Color gradients represent local variations in shear stress intensity by nm/nm, with warmer colors indicating regions of elevated interfacial stress.

Table 3 summarized shear stress on cell membrane domain for imposed velocities to water molecules

Water molecules velocity (m/s)	Computed Wall Shear Stress (Pa)
0.5	8.77
1	14.6
1.5	27.49
5	33.4

"Figures 8-b" shows a planar view of the POPC lipid bilayer highlighting the spatial distribution of shear strain at t = 200 picoseconds, in which water molecules were driven across the membrane surface at a velocity of 0.5 m/s from right to left. For clarity, water molecules were removed from the visualization, isolating the membrane response. The color scale represents the local shear strain experienced by lipid molecules, with cooler tones (blue) indicating regions of lower strain and warmer tones (yellow to red) denoting areas of higher deformation. The strain distribution exhibits significant heterogeneity across the membrane surface. Higher shear strain concentrations, particularly in the rightmost and lower-right regions, correspond to areas directly impacted by the initial fluid–membrane interaction, where momentum transfer from the sheared water molecules is most intense.

Comparing the contour plots for fluid velocities of 1 m/s and 5 m/s reveals significant differences in shear strain distribution within the POPC membrane. In "Figure 8-c", the shear strain is relatively moderate, with variations observed primarily in localized regions due to fluid interaction. Lower shear strain areas remain relatively stable, indicating minimal lipid displacement. The contour plot exhibits higher strain regions, where the deformation is more pronounced, suggesting that elevated fluid velocity enhances lipid displacement and membrane remodeling. The differences in strain distribution between the two cases highlight the nonlinear relationship between fluid shear and membrane mechanics. The higher velocity (5 m/s) imposes greater shear stress, increasing deformation across the membrane surface and potentially affecting lipid organization, membrane permeability, and structural integrity. This observation aligns with biomechanical studies demonstrating that shear forces influence lipid dynamics in biological membranes.

"Figure 8-d and 8-e" present the distribution of shear strain within the POPC cell membrane subjected to fluid shear stress. The membrane was exposed to a fluid velocity of 1.5, 5 m/s, flowing from right to left, leading to differential strain patterns across the membrane surface. As the water molecules exert shear forces on the membrane, localized strain accumulates, potentially impacting lipid arrangement and membrane stability. The visualization is captured at 200 picoseconds to provide insight into the temporal progression of strain response in the lipid bilayer. Higher strain regions suggest pronounced lipid displacement due to sustained fluid interaction, while lower strain areas imply relative stability in those regions.

The observed strain distribution in "Figures 8" aligns with the findings from "Figure 7", reinforcing that increased fluid velocity enhances lipid displacement and membrane remodeling. These insights contribute to the understanding of membrane biomechanics and its implications for biological membranes, synthetic lipid systems, and fluid-induced structural adaptations. Summarized values of shear stresses relevant to water velocities ("Figure 7") are reported in "Table 3" as well.

4-Conclusions

In common MD simulations there are time scale and box size limitations. As the box size increases number of interacting molecules increase as well. This leads to significant increase in simulation time. By increasing the time scale of the simulations (in order of tens of nanoseconds) this problem uprises again. This study examined the interaction between water, the dominant fluid in the human body and a lipid bilayer (POPC) subjected to varying velocity ranges. Every single simulation conducted in this study, took 15 hours with 4 engaged processors simultaneously.

By employing molecular dynamics simulations, the effects of shear forces on membrane mechanics were investigated, with a particular emphasis on their implications for drug delivery systems. Water molecules were applied to the membrane at velocities ranging from 0.5 m/s to 5 m/s, allowing for the quantification of shear strain and shear stress across different conditions. The results demonstrated a clear correlation between increasing tangential velocity and enhanced shear strain within the membrane, suggesting potential alterations in permeability and molecular transport mechanisms essential for biological processes.

Additionally, the study analyzed the impact of fluid shear stress by calculating averaged values across the membrane plane. It was observed that as velocity increased, the shear stress approached the permissible limit for different blood vessel types. This finding underscores the importance of regulating fluid forces to maintain membrane integrity under physiological conditions. Notably, at a velocity of 5 m/s, shear stress values reached critical levels, nearing the structural threshold beyond which membrane rupture could occur. Such extreme conditions have direct implications for vascular biomechanics, as excessive shear stress may compromise membrane stability and disrupt essential cellular functions, particularly in circulatory environments exposed to fluctuating hemodynamic forces. The insights gained from this study provide valuable contributions to the understanding of membrane biomechanics under fluidic shear conditions. By elucidating the relationship between tangential velocity, shear strain, and shear stress, this research reinforces the necessity of optimizing fluid interactions in biomedical applications, including targeted drug delivery and vascular health assessments. Future investigations may extend this analysis by incorporating additional lipid compositions, fluid properties, and physiological parameters to enhance the predictive accuracy of membrane behavior under dynamic conditions. Such advancements could lead to improved drug transport models, better therapeutic strategies, and a deeper understanding of membrane resilience in complex biological systems.

Ethical Statement

The content of this manuscript is original, based on the authors' research, and has not been published or submitted elsewhere, either in Iranian or international journals.

Conflict of intrest

The authors declared that they have no conflicts of interest to this work.

References

[1] P. R. Byron, "Drug delivery devices: Issues in drug development," Proceedings of the American Thoracic Society, vol. 1, pp. 321–328, 2004. doi: http://doi.org/10.1513/pats.2306038.

[2] M. Epshtein and N. Korin, "Shear targeted drug delivery to stenotic blood vessels," Biomechanics, vol. 1, pp. 217–221, 2016. doi: http://doi.org/10.3390/biomechanics1010017.

[3] M. J. Thubrikar and F. Robicsek, "Pressure-induced arterial wall stress and atherosclerosis," Hypertension, vol. 26, pp. 1594–1602, 1995. doi: http://doi.org/10.1161/01.HYP.26.6.1594.

[4] S. Mishani, H. Belhoul-Fakir, C. Lagat, S. Jansen, B. Evans, and M. Lawrence-Brown, "Stress distribution in the walls of major arteries: Implications for atherogenesis," Quantitative Imaging in Medicine and Surgery, vol. 11, pp. 3494–3505, 2021. doi: http://doi.org/10.21037/qims-20-1035.

[5] A. R. Ahlgren, M. Cinthio, H. W. Persson, and K. Lindström, "Targeted drug delivery to flow-obstructed blood vessels using mechanically activated nanotherapeutics," Ultrasound in Medicine and Biology, vol. 38, pp. 916–925, 2012. doi: http://doi.org/10.1016/j.ultrasmedbio.2011.12.004.

[6] N. Korin, M. J. Gounis, A. K. Wakhloo, and D. E. Ingber, "Targeted drug delivery to flow-obstructed blood vessels using mechanically activated nanotherapeutics," Science, vol. 345, pp. 1148–1151, 2014. doi: http://doi.org/10.1126/science.1250322.

[7] N. Hosseinkhah, D. E. Goertz, and K. Hynynen, "Microbubbles and blood-brain barrier opening: A numerical study on acoustic emissions and wall stress predictions," IEEE Transactions on Biomedical Engineering, vol. 62, no. 5, pp. 1293–1304, May 2015. doi: http://doi.org/10.1109/TBME.2014.2385651.

[8] J. Venugopal, M. P. Prabhakaran, S. Low, A. T. Choon, G. Deepika, V. R. G. Dev, and S. Ramakrishna, "Continuous nanostructures for the controlled release of drugs," Current Pharmaceutical Design, vol. 15, no. 15, pp. 1799–1808, 2009. doi: http://doi.org/10.2174/138161209788682318.

[9] M. N. V. Ravi Kumar and N. Kumar, "Polymeric controlled drug-delivery systems: perspective issues and opportunities," Drug Development and Industrial Pharmacy, vol. 27, no. 1, pp. 1–30, 2001. doi: http://doi.org/10.1081/DDC-100000124.

[10] Y. K. Sung and S. W. Kim, "Recent advances in polymeric drug delivery systems," Biomaterials Research, vol. 24, no. 1, p. 12, 2020. doi: http://doi.org/10.1186/s40824-020-00190-7.

[11] T. M. Allen and P. R. Cullis, "Liposomal drug delivery systems: From concept to clinical applications," Advanced Drug Delivery Reviews, vol. 65, no. 1, pp. 36–48, January 2013. doi: http://doi.org/10.1016/j.addr.2012.09.037.

[12] L. Zhang, D. Pornpattananangkul, C.-M. J. Hu, and C.-M. Huang, "Development of nanoparticles for antimicrobial drug delivery," Current Medicinal Chemistry, vol. 17, no. 6, pp. 585–594, 2010. doi: http://doi.org/10.2174/092986710790416290.

[13] Y. H. Choi and H.-K. Han, "Nanomedicines: current status and future perspectives in aspect of drug delivery and pharmacokinetics," Journal of Pharmaceutical Investigation, vol. 48, no. 1, pp. 43–60, January 2018. doi: http://doi.org/10.1007/s40005-017-0370-4.

[14] R. Kadian, "Nanoparticles: A promising drug delivery approach," Asian Journal of Pharmaceutical and Clinical Research, vol. 11, no. 1, pp. 1–5, 2018. doi: http://doi.org/10.22159/ajpcr.2018.v11i1.22035.

[15] S. Singh, V. K. Pandey, P. R. Tewari, and V. Agarwal, "Nanoparticle based drug delivery system: Advantages and applications," Indian Journal of Science and Technology, vol. 4, pp. 177–180, 2011. doi: http://doi.org/10.17485/ijst/2011/v4i3/29910.

[16] H. K. Sajja, M. P. East, H. Mao, Y. A. Wang, S. Nie, and L. Yang, "Development of multifunctional nanoparticles for targeted drug delivery and noninvasive imaging of therapeutic effect," Current Drug Discovery Technologies, vol. 6, no. 1, pp. 43–51, March 2009. doi: http://doi.org/10.2174/157016309787581066.

[17] R. W. Pastor and A. D. Mackerell, "Development of the CHARMM Force Field for Lipids," The Journal of Physical Chemistry B, vol. 115, no. 6, pp. 1526-1532, 7 June 2011. doi: http://doi.org/10.1021/jp101759q.

[18] K. Murzyn, T. Róg, G. Jezierski, Y. Takaoka, and M. Pasenkiewicz-Gierula, "Effects of phospholipid unsaturation on the membrane/water interface: A molecular simulation study," Biophysical Journal, vol. 81, no. 1, pp. 170–183, 2001. doi: http://doi.org/10.1016/S0006-3495(01)75689-5.

[19] F. Sotoudeh, A. Rajabpour, and M. Khanaki, "Shock wave propagation in the solid argon by molecular dynamics simulation: Effect of initial strain," Modares Mechanical Engineering, vol. 16, no. 3, pp. 364–370, 2016. [Online]. Available: lire.modares.ac.ir.

[20] B. Afshari and M. Rostami Varnousfaaderani, "Numerical investigation of cavitation effect on the performance of waterjet propulsion system by computational fluid dynamics," Modares Mechanical Engineering, vol. 19, no. 7, pp. 1788–1779, 2019. [Online]. Available: lire.modares.ac.ir.

[21] C.-D. Ohl and B. Wolfrum, "Detachment and sonoporation of adherent HeLa cells by shock wave-induced cavitation" Biochimica et Biophysica Acta (BBA) - General Subjects, vol. 1624, pp. 131–138, 2003. doi: http://doi.org/10.1016/j.bbagen.2003.10.005.

[22] Z. Heidary, C.-D. Ohl, and A. Mojra, "Numerical analysis of ultrasound-mediated microbubble interactions in vascular systems: Effects on shear stress and vessel mechanics." Physics of Fluids 36, 081903, 2024. doi: http://doi.org/10.1063/5.0213656.

[23] Z. Heidary, Y. Fan, A. Mojra, and C.-D. Ohl, " Robust cavitation-based pumping into a capillary" Physics of Fluids 36, 123335, 2024. doi: http://doi.org/10.1063/5.0238826.

[24] M. Vedadi, A. Choubey, K. Nomura, R. K. Kalia, A. Nakano, P. Vashishta, and A. C. T. van Duin, "Structure and Dynamics of Shock-Induced Nanobubble Collapse in Water" Physical Review Letters, vol. 105, no. 1, p. 014503, 2010. doi: http://doi.org/10.1103/PhysRevLett.105.014503.

[25] D. D. Sun, X. Lin, Z. Zhang, and N. Gu, "Impact of Shock-Induced Lipid Nanobubble Collapse on a Phospholipid Membrane," Journal of Physical Chemistry C, vol. 120, no. 33, pp. 18803–18810, 2016. doi: http://doi.org/10.1021/acs.jpcc.6b04086.

[26] N. Nan, D. Si, and G. Hu, "Nanoscale cavitation in perforation of cellular membrane by shock-wave induced nanobubble collapse," The Journal of Chemical Physics, vol. 149, no. 7, p. 074701, 2018. doi: http://doi.org/10.1063/1.5037643.

[27] E. Ebrahimi and A. Pishevar, "Dependence of the Dynamics of Spontaneous Imbibition into Carbon Nanotubes on the Strength of Molecular Interactions," Physical Chemistry C, vol. 119, no. 49, pp. 28389–28395, 15 December 2015. doi: http://doi.org/10.1021/acs.jpcc.5b08637.

[28] C. M. Otto, "Valvular aortic stenosis: disease severity and timing of intervention," Journal of the American College of Cardiology, vol. 47, no. 11, pp. 2141-2151, 15 May 2006. doi: http://doi.org/10.1016/j.jacc.2006.03.002.